Available online at www.eccomasproceedia.org
Eccomas Proceedia SMART (2023) 191-202

ECCOMAS
Proceedia

X ECCOMAS Thematic Conference on Smart Structures and Materials
SMART 2023
D.A. Saravanos, A. Benjeddou, N. Chrysochoidis and T. Theodosiou (Eds)

ANALYSIS AND TUNING OF MULTIPLE SHUNTED PIEZOELECTRIC TRANSDUCERS

Jens D. Richardt*, Jan Høgsberg*, Boris Lossouarn† and Jean-François Deü†

*Technical University of Denmark, Kongens Lyngby, Denmark

† Conservatoire national des arts et métiers (Cnam), HESAM université, F 75003, Paris, France

Key words: Piezoelectric shunt damping, shunt calibration, residual mode correction, electromechanical coupling coefficient, multiple shunt correction, smart structures

Abstract. Piezoelectric RL shunts are resonant devices that require accurate tuning for efficient vibration reduction of a targeted vibration mode. Anti-resonance can occur at the target frequency when multiple shunts are tuned individually to the same frequency. The system description in the present paper consistently includes the coupling between multiple shunts targeting the same vibration mode. This enables the formulation of a balanced tuning for each shunt, which accounts for the combined influence from the other shunts. The ability of the present system description to achieve effective multi-shunt damping is demonstrated by a numerical example with five parallel RL shunts attached to a cantilever beam.

1 INTRODUCTION

Passive shunts have been used for vibration mitigation since the introduction by Forward in 1979 [1]. Significant vibration reduction of a target frequency can be obtained using resonant RL (resistive-inductive) shunts. In the resonant shunt, an inductance L and resistance R are tuned with the capacitance C of the piezoelectric transducer to obtain electrical resonance with the targeted structural resonance frequency. If the shunt is tuned correctly, the electrical resonance allows for large energy dissipation by the resistance. The tuning of single resonant shunts usually refers back to the tuning by Hagood and von Flotow [2] for series RL shunts and to the tuning by Wu in [3] for parallel RL shunts. Other tuning methods have since been introduced for resonant shunts with different objectives [4].

The tuning of resonant vibration absorbers can be sensitive to changes in the parameters affecting the resonant frequency. The shunt calibration is typically based on a single-degree-of-freedom (sdof) approximation, which has been extended recently to correct for the influence from residual modes [5, 6]. When multiple piezoelectric shunts target a single vibration mode, their individual contributions might lead to an unbalanced tuning when using the pure sdof calibration expressions that do not account for the influence from the other shunts. While there are several articles on multiple piezoelectric shunts targeting multiple vibration modes, there

Peer-review under responsibility of the organizing committee of SMART 2023.
doi: 10.7712/150123.9777.444070

seems to be little to no literature available on the modelling and tuning of multiple piezoelectric shunts targeting a single vibration mode.

The present paper aims at developing general modal expressions that allow for stiffness correction for the non-targeted modes in the individual tuning of multiple shunts targeting a single vibration mode. The stiffness correction can be described in terms of the modal electromechanical coupling coefficient (EMCC), whereby it can potentially be estimated experimentally or numerically by solving the corresponding eigenvalue problems.

A simplified tuning approach is presented for the parallel RL shunt and applied to a cantilever beam with five shunts to investigate the influence of the stiffness correction in the tuning of each shunt. The simplified tuning approach is based on the tuning of a single parallel RL-shunt in [7] with a stiffness correction from the other shunts. It is shown that this approach leads to balanced tuning for the cantilever beam, similar to when a single RL shunt is used alone.

The present paper is divided into four sections. In Section 2, a general system description is presented for a beam with multiple piezoelectric shunts targeting the same vibration mode. The description includes a force-displacement relationship for each shunt, including the influence from all other shunts described in terms of the modal EMCC. In Section 3, a simplified tuning approach is presented to allow for balanced shunt tuning of the five parallel RL shunts acting on the cantilever. The tuning is compared to the individual tuning of the shunts in Section 4 to illustrate the effect of correcting for the other shunts in the tuning of a single shunt. Finally, the main results are discussed in Section 5 along with the limitations of the present work and some future perspectives.

2 SYSTEM DESCRIPTION

Multiple piezoelectric shunts can be attached to a structure and tuned to increase the damping of one or more vibration modes. This section describes a general electromechanical system in a format that allows for tuning of the attached piezoelectric shunts to a single target mode.

2.1 Governing structural equations

The current paper is based on an analysis of the cantilever beam in Figure 1 with $N_p = 5$ piezoelectric shunts attached. The beam has a length 0.4 m, stiffness $EI = 7.875\,\mathrm{Nm}^2$, and mass per unit length $\rho A = 0.4155\,\mathrm{kg/m}$. The beam is modelled with 24 elements, with one translational and one rotational degree of freedom (dof) per node. Shear deflection is neglected, whereby the element mass- and stiffness matrices are equal to the ones given in Section 5.3.3. in [8]. The piezoelectric shunts are each placed between two nodes, and the axial force from each piezoelectric laminate is not included. Thereby, the generalized force acting on the structure can be described as a moment pair with magnitude $f_{0,n}$ for shunt n. The governing equation of motion can then be written in the discretized form

$$\left(-\omega^2\mathbf{M}_0 + \mathbf{K}_0\right)\mathbf{q} + \sum_{n=1}^{N_p} \mathbf{w}_n f_{0,n} = \mathbf{f}_{\text{ext}} \tag{1}$$

where $\mathbf{M}_0$ and $\mathbf{K}_0$ are the mass and stiffness matrix of the structure, respectively. The angular frequency is ω, $\mathbf{q}$ is the nodal displacement vector and $\mathbf{f}_{\text{ext}}$ is the external load vector. The location of the moment pair $f_{0,n}$ is defined by a connectivity vector $\mathbf{w}_n$ with positive and

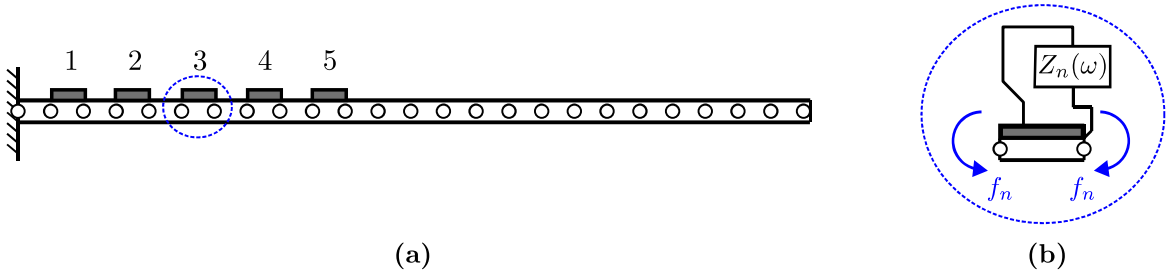

Figure 1: (a) Cantilever beam with five piezoelectric shunts. (b) Moment pair f_n for shunt n.

negative unit entries for the corresponding dof. The connectivity vector for the shunt closest to the support is thereby constructed as

$$\mathbf{w}_1^T = [0\,,\,0\,,\,0\,,\,1\,,\,0\,,\,-1\,,\,0\,,\,0\,,\,\ldots\,,\,0]^T \tag{2}$$

In the following, n refers to the number of the shunted piezoelectric transducer on the beam.

The force acting on the structure from each shunt $f_{0,n}$ can be defined in terms of the voltage V_n and generalized displacement $\mathbf{w}_n^T\mathbf{q}$ (change in rotation) across the transducer [9]

$$f_{0,n} = \theta_n V_n + K_a \mathbf{w}_n^T \mathbf{q} \tag{3}$$

where θ_n is a proportionality factor relating V_n and $f_{0,n}$ in case of constant strain, while K_a is the mechanical stiffness of the piezoelectric transducer with short circuited (SC) electrodes. It is convenient to include K_a in the equation of motion by introducing $\mathbf{K} = \mathbf{K_0} + K_a \mathbf{w}_n \mathbf{w}_n^T$ in (1), while the mass of the piezoelectric transducers is neglected, i.e. $\mathbf{M} = \mathbf{M}_0$. The governing structural equation of motion is then given as

$$\left(-\omega^2 \mathbf{M} + \mathbf{K}\right) \mathbf{q} + \sum_{n=1}^{N_p} \mathbf{w}_n f_n = \mathbf{f}_{\text{ext}} \tag{4}$$

in which the corresponding control force from each piezoelectric shunt

$$f_n = \theta_n V_n \tag{5}$$

is proportional to the respective shunt voltage V_n.

2.2 Force-displacement relationship

Each piezoelectric transducer can be connected to any electric circuit, represented by the frequency-dependent impedance $Z_n(\omega)$ relating the voltage V_n across the transducer to its current I_n. The equivalent electric circuit of a piezoelectric shunt with a current source is illustrated in Figure 2(a). The current I_n is related to the charge Q_n by $I_n = i\omega Q_n$, whereby

$$V_n = -Z_n(\omega) I_n = -i\omega Z_n(\omega) Q_n \tag{6}$$

From [9], the balance or sensor equation is defined for each piezoelectric transducer by

$$Q_n = -\theta_n \mathbf{w}_n^T \mathbf{q} + C_n V_n \tag{7}$$

Figure 2: Piezoelectric shunt with: (a) Equivalent electric circuit. (b) Equivalent mechanical model.

where C_n is the capacitance of the piezoelectric transducer in case of constant strain. Inserting (5) and (6) into the balance equation in (7) leads to the following relation between the force f_n and deformation $\mathbf{w}_n^T\mathbf{q}$ along the piezoelectric transducer,

$$\left(\frac{C_n}{\theta_n^2} + \frac{1}{i\omega\theta_n^2 Z_n(\omega)}\right) f_n = \mathbf{w}_n^T\mathbf{q} \tag{8}$$

An equivalent mechanical model with the same force-displacement relationship is shown in Figure 2(b). The capacitance C_n of the piezoelectric transducer corresponds to a mechanical spring θ_n^2/C_n, while the frequency-dependent impedance $Z_n(\omega)$ corresponds to the frequency-dependent damping term $Z_n(\omega)\theta_n^2$. From this direct electromechanical analogy, the parallel components in the electric circuit correspond to components in series in the equivalent mechanical model [10].

2.3 Modal expansion

A modal expansion is applied for the structure with all shunts in SC, whereby $V_n = 0$ across a shunt in SC corresponds to a vanishing impedance ($Z_n(\omega) = 0$). It then follows directly from (8) that the SC condition implies $f_n = 0$ so that the associated eigenvalue problem

$$\left(-\omega_j^2\mathbf{M} + \mathbf{K}\right)\mathbf{u}_j = \mathbf{0} \tag{9}$$

defines ω_j as the natural frequency and $\mathbf{u}_j$ as the mode-shape vector for mode j.

The structure response can be expressed in terms of the N modes by the modal expansion

$$\mathbf{q} = \sum_{j=1}^{N} \mathbf{u}_j r_j \tag{10}$$

which introduces r_j as the modal coordinate. The modal expansion in (10) is inserted into the force-displacement relation in (8), which yields the modal force-displacement relation

$$\left(\frac{C_n}{\theta_n^2} + \frac{1}{i\omega\theta_n^2 Z_n(\omega)}\right) f_n = \sum_{j=1}^{N} \nu_{j,n} r_j \tag{11}$$

in which the relative change in mode j across shunt n is defined as

$$\nu_{j,n} = \mathbf{u}_j^T\mathbf{w}_n = \mathbf{w}_n^T\mathbf{u}_j \tag{12}$$

When pre-multiplying the governing equation of motion (4) with $\mathbf{u}_j^T$ and inserting the modal expansion from (10), the resulting modal equation can be written as

$$\left(-\omega^2 m_j + k_j\right) r_j + \sum_{n=1}^{N_p} \nu_{j,n} f_n = f_{\text{ext},j} \tag{13}$$

with the modal mass m_j, modal stiffness k_j and modal load $f_{\text{ext},j}$ defined as

$$m_j = \mathbf{u}_j^T \mathbf{M} \mathbf{u}_j \quad , \quad k_j = \mathbf{u}_j^T \mathbf{K} \mathbf{u}_j \quad , \quad f_{\text{ext},j} = \mathbf{u}_j^T \mathbf{f}_{\text{ext}} \tag{14}$$

Note that no assumptions are made regarding the normalization of the mode-shape vectors.

2.4 Modal truncation

A modal truncation of the residual vibration modes can increase the accuracy of the tuning compared to an sdof approximation, see e.g. [6, 5]. In the current paper, a modal truncation is introduced to include the higher modes for all shunts. The truncation is introduced to take all shunts into account in the tuning of each shunt. The piezoelectric shunts are tuned to a single target mode s, whereby it is convenient to separate the deformation along the piezoelectric transducer n on the right-hand side in (11) into a modal deformation from target mode s and the deformation of residual modes ($j \neq s$). Thus, the modal summation can be expressed as

$$\sum_{j=1}^{N} \nu_{j,n} r_j = \nu_{s,n} r_s + \sum_{j \neq s}^{N} \nu_{j,n} r_j \tag{15}$$

The modal coordinate r_j for the residual modes $j \neq s$ is determined from (13) for the case of free vibrations with $f_{\text{ext},j} = 0$. When the modal coordinate is inserted into (15) and the relation $\omega_j^2 = k_j/m_j$ for the natural frequency is used, the total modal deformation can be expressed as

$$\sum_{j=1}^{N} \nu_{j,n} r_j = \nu_{s,n} r_s - \sum_{j \neq s}^{N} \nu_{j,n} \frac{\sum_{m=1}^{N_p} \nu_{j,m} f_m}{-\omega^2 m_j + k_j} = \nu_{s,n} r_s + \sum_{m=1}^{N_p} \sum_{j \neq s}^{N} \frac{\nu_{j,n} \nu_{j,m}}{k_j} \frac{\omega_j^2}{\omega^2 - \omega_j^2} f_m \tag{16}$$

The summation of residual modes $j \neq s$ is separated into a summation of lower and higher vibration modes, corresponding to $j < s$ and $j > s$, respectively. If the natural frequencies are well separated, it follows for frequencies ω near the target frequency ω_s that $\omega \gg \omega_j$ for the lower vibration modes. In this case, the term $\omega_j^2/(\omega^2 - \omega_j^2)$ tends towards zero and the influence from the lower vibration modes is neglected. Similarly, for the higher vibration modes $\omega \ll \omega_j$ whereby $\omega_j^2/(\omega^2 - \omega_j^2) \approx -1$. Using these approximations for lower and higher modes, the modal truncation in (16) is significantly reduced as

$$\sum_{j=1}^{N} \nu_{j,n} r_j \approx \nu_{s,n} r_s - \sum_{m=1}^{N_p} \sum_{j>s}^{N} \frac{\nu_{j,n} \nu_{j,m}}{k_j} f_m \tag{17}$$

where the double summation contains the residual effect from all shunts. The truncation in (17) is inserted into the force-displacement relationship for shunt n in (11), leading to

$$\left(\frac{k_s C_n}{\theta_n^2} + \frac{k_s}{i\omega \theta_n^2 Z_n(\omega)} \right) \frac{f_n}{k_s} + \sum_{m=1}^{N_p} \sum_{j>s}^{N} \nu_{j,n} \nu_{j,m} \frac{k_s}{k_j} \frac{f_m}{k_s} = \nu_{s,n} r_s \tag{18}$$

The right side in (18) contains the modal response of the structure, while the left side contains the force from shunt n and the correction for higher residual modes.

2.5 Normalized parameters

In this section, the force-displacement relationships in (18) and the modal equation in (13) are written in normalized form. The natural frequency of the target mode s is defined as $\omega_{sc} = \omega_s$ to highlight that the modal expansion represents all shunts in SC, whereby a non-dimensional frequency for target mode $j = s$ is conveniently introduced as

$$\rho = \frac{\omega}{\omega_{sc}} = \frac{\omega}{\omega_s} \tag{19}$$

When introducing a Kronecker delta δ_{nm}, the normalized relation in (18) for shunt n becomes

$$\sum_{m=1}^{N_p} \left(\frac{1}{\tilde{\kappa}_{nm}} + \frac{1}{i\rho} \frac{1}{\beta_{nm}(\rho)} \right) \tilde{f}_m = r \tag{20}$$

with the corresponding modal structural equation for free vibrations

$$\left(1 - \rho^2\right) r + \sum_{m=1}^{N_p} \tilde{f}_m = 0 \tag{21}$$

introducing the normalized parameters

$$\frac{1}{\tilde{\kappa}_{nm}} = \delta_{nm} \frac{k_s C_n}{\nu_n^2 \theta_n^2} + \sum_{j>s}^{N} \frac{\nu_{j,n} \nu_{j,m}}{\nu_n \nu_m} \frac{k_s}{k_j} \quad , \quad \frac{1}{\beta_{nm}(\rho)} = \delta_{nm} \frac{k_s}{\omega_{sc} \nu_n^2 \theta_n^2 Z_n(\rho \omega_{sc})} \quad , \quad \tilde{f}_m = \frac{\nu_m f_m}{k_s} \tag{22}$$

The relative change in the target mode s across shunt n is defined as $\nu_n = \nu_{s,n}$ and the modal coordinate is defined as $r = r_s$. The effective and symmetric stiffness parameter $1/\tilde{\kappa}_{nm}$ contains the modal truncation of the non-targeted modes. In the case where $m = n$, the term $1/\tilde{\kappa}_{nm}$ also contains the added non-dimensional mechanical stiffness $k_s C_n / (\nu_n^2 \theta_n^2)$ for shunt n in its open circuit (OC) limit. The non-dimensional damping parameter $1/\beta_{nn}(\rho)$ corresponds to the shunt impedance of shunt n, while the term $\tilde{f}_m$ is the normalized control force for shunt m.

2.6 Effective stiffness

The effective stiffness parameter $1/\tilde{\kappa}_{nm}$ can be obtained directly from the modal electromechanical coupling coefficient (EMCC) for pairs of shunts in OC with all other shunts in SC. Although the detailed derivation is outside the scope of the current paper, the compact expression for the modal EMCC is conveniently expressed in reciprocal form as

$$\frac{1}{\tilde{\kappa}_{nm}} = \frac{1}{K_{c,nm}^2} - \frac{1}{K_{c,nm}^2} \sqrt{\left(\frac{K_{c,nm}^2}{K_{c,n}^2} - 1 \right) \left(\frac{K_{c,nm}^2}{K_{c,m}^2} - 1 \right)} \tag{23}$$

where $K_{c,nm}^2$ is the EMCC with the shunts n and m in OC and all other shunts in SC. Similarly, $K_{c,n}^2$ is the EMCC for the shunt n in OC and all other shunts in SC. For $n = m$, the component

$\tilde{\kappa}_{nn}$ corresponds to the EMCC with shunt n in OC and all other shunts in SC. Note that the definition of the EMCC corresponds to the one used in e.g. [2, 9], whereby

$$K^2_{c,nm} = \frac{\omega^2_{oc,nm} - \omega^2_{sc}}{\omega^2_{sc}} \tag{24}$$

where $\omega_{oc,nm}$ is the natural frequency with shunts n and m in OC, and all other shunts in SC.

3 SHUNT TUNING

The force-displacement relationships in (20) and the corresponding modal equation in (21) enable the tuning of multiple decentralized shunts to target the same vibration mode, while taking the influence of the residual modes from all shunts into account. The coupling is based on the modal truncation of the non-targeted vibration modes in $1/\tilde{\kappa}_{nm}$ for $n \neq m$. A simple tuning procedure that balances multiple parallel RL shunts is presented in the following.

3.1 Decoupling of equations

A characteristic equation for the decentralized shunts can be obtained by writing (20) and (21) on matrix form and isolating the vector with $\tilde{f}_n$. However, this requires inverting a fully populated $N_p \times N_p$ matrix, complicating the use of this equation for explicit shunt tuning.

In a balanced design, the forces f_k imposed by the shunts are expected to be of the same order of magnitude around the target frequency ω_{sc} for mode $j = s$. The shunts are typically placed to have a significant effect on the targeted vibration mode. It is expected that the normalized forces $\tilde{f}_k$ are also of the same order of magnitude, even though $\tilde{f}_k$ are scaled by the relative change ν_k in the target mode-shape along each shunt. From (20) and (21) it is seen directly that the assumption $\tilde{f}_1 = \tilde{f}_2 = \cdots = \tilde{f}_{N_p}$ results in a significant simplification, which gives the characteristic equation for tuning of shunt n in the compact form

$$\rho^2 - 1 = \frac{N_p}{\dfrac{1}{\hat{\kappa}_n} + \dfrac{1}{i\rho}\dfrac{1}{\beta_{nm}}} \tag{25}$$

where $1/\hat{\kappa}_n = \sum_m 1/\tilde{\kappa}_{nm}$ represents the sum of all reciprocal contributions to the specific shunt.

The simplification $\tilde{f}_1 = \tilde{f}_2 = \cdots = \tilde{f}_{N_p}$ leads to a decoupled characteristic equation for shunt n with a correction for the capacitance of the other shunts in the term $1/\hat{\kappa}_n$. By the introduction of the corrected single-shunt characteristic equation in (25), it is now possible to use a standard tuning approach for a single shunt and still include a correction for the influence from all other shunts attached to the structure.

3.2 Tuning of individual shunts

The tuning is summarized for a parallel RL shunt to illustrate the individual tuning of each shunt based on the characteristic equation in (25). The equivalent electrical circuit and mechanical model are shown in Figure 3 with the resistance R_n and inductance L_n. It is convenient to use a calibration based on root locus analysis as this allows root locus plots to be used to evaluate the tuning when multiple shunts act simultaneously. Only the main steps

are shown here as the tuning method is presented in [5] with modal inductance and resistance from [7].

The characteristic equation in (25) can be rewritten as the cubic polynomial

$$\rho^4 - i\rho^3 \frac{\hat{\kappa}_n}{\beta_{nn}} - \rho^2 \left(N_p \hat{\kappa}_n + 1\right) + i\rho \frac{\hat{\kappa}_n}{\beta_{nn}} = 0 \tag{26}$$

The reciprocal form of the impedance for the parallel RL shunt is given as

$$\frac{1}{Z_n(\rho\omega_{sc})} = \frac{1}{R_n} + \frac{1}{i\rho\omega_{sc} L_n} \tag{27}$$

in which it is used that angular frequency $\omega = \rho\omega_{sc}$. By inserting (27) into the definition of $1/\beta_{nm}(\rho)$ in (22) and then substituting the expression into (26), the governing quartic characteristic equation can be written in normalized form as

$$\rho^4 - i\rho^3 \frac{\hat{\kappa}_n k_s}{\omega_{sc}\nu_n^2\theta_n^2 R_n} - \rho^2 \left(\frac{\hat{\kappa}_n k_s}{\omega_{sc}^2\nu_n^2\theta_n^2 L_n} + N_p\hat{\kappa}_n + 1\right) + i\rho \frac{\hat{\kappa}_n k_s}{\omega_{sc}\nu_n^2\theta_n^2 R_n} + \frac{\hat{\kappa}_n k_s}{\omega_{sc}^2\nu_n^2\theta_n^2 L_n} = 0 \tag{28}$$

A balanced tuning is obtained when the two complex roots from (28) in the positive Re[ω]-plane meet at a bifurcation point ρ_*, which corresponds to maximum damping. This is illustrated in Figure 4(a) for tuning of the shunt closest to the support in Figure 1 with respect to the first mode $s = 1$ as target and all other shunts in SC. Following the outline in [11], this balanced tuning is obtained by comparison of (28) with the generic polynomial

$$\rho^4 - i\rho^3 4\,\mathrm{Im}(\rho_*) - \rho^2\left(2|\rho_*|^2 + 4\,\mathrm{Im}(\rho_*)^2\right) + i\rho 4\,\mathrm{Im}(\rho_*)|\rho_*|^2 + |\rho_*|^4 = 0 \tag{29}$$

Comparison of odd-power terms lead to expressions for $4\,\mathrm{Im}(\rho_*)$ and $|\rho_*|^2$, which are used in the comparison of constant and quadratic terms to obtain expressions for inductance and resistance,

$$L_n = \frac{\hat{\kappa}_n k_s}{\omega_{sc}^2\nu_n^2\theta_n^2} \quad , \quad R_{*,n} = \frac{1}{2\sqrt{N_p}} \frac{\sqrt{\hat{\kappa}_n} k_s}{\omega_{sc}\nu_n^2\theta_n^2} \tag{30}$$

where the asterisk $(*)$ denotes that the resistance is associated with the bifurcation point.

As described in [7], the bifurcation point ρ_* corresponds to maximum modal damping. However, constructive interference occurs when the two roots are identical. This yields an undesirable peak in the structural frequency response function (FRF), as illustrated in Figure 4(b) for the

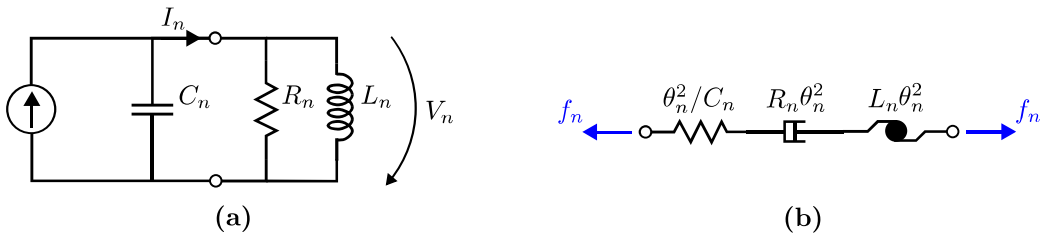

Figure 3: Parallel RL shunt with: (a) Equivalent electric circuit. (b) Equivalent mechanical model.

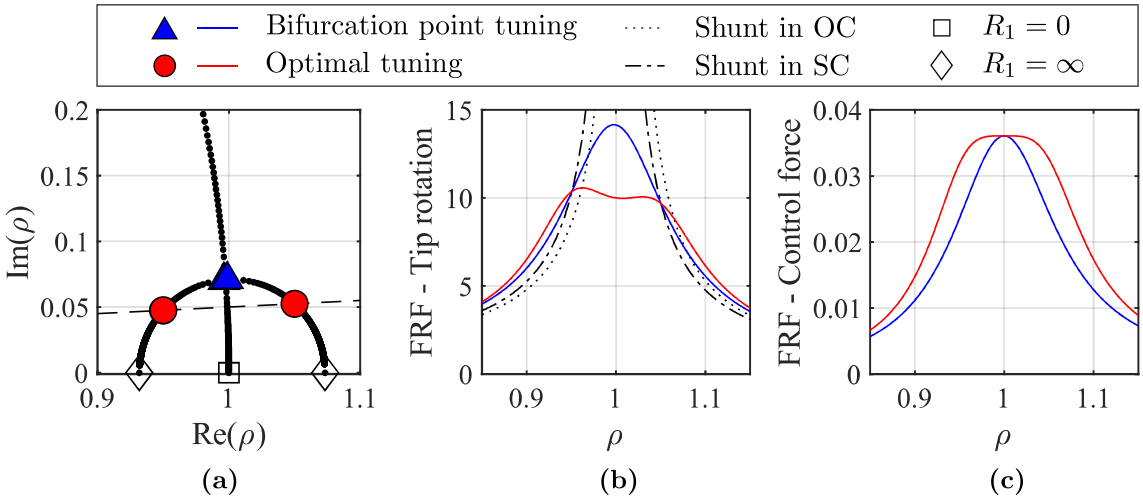

Figure 4: Tuning of a single parallel RL shunt: (a) Root locus diagram with varying resistance. (b),(c) FRF for the resistance corresponding to the bifurcation point (blue) and for the optimal resistance (red).

shunt closest to the root in Figure 1. The FRF is created by the external load vector $\mathbf{f} = \mathbf{M}\mathbf{u}_s$, which by mass orthogonality must vanish for all other vibration modes ($j \neq s$). A suitable tuning can be obtained by increasing the resistance by $\sqrt{2}$ for the parallel RL shunt, which leads to the optimal resistance

$$R_n = \sqrt{2}R_{*,n} = \frac{\sqrt{2}}{2\sqrt{N_p}} \frac{\sqrt{\tilde{\kappa}_n} k_s}{\omega_{sc} \nu_n^2 \theta_n^2} \tag{31}$$

that creates equal roots sufficiently below the bifurcation point to avoid interference. When a single shunt is used, then $N_p = 1$ and the resistance in (31) corresponds to the optimal resistance originally derived by Wu in [3] for a single parallel RL shunt. As shown in Figure 4, the increased parallel resistance leads to a nearly flat plateau in the FRF (b) and a fully flat plateau in the force amplitude for f_1 in (c).

4 EXAMPLE OF APPLICATION

The balanced tuning of the shunts is implemented for the cantilever beam in Figure 1 with five shunts. All shunts are tuned with respect to the target mode $s = 1$. The capacitance C_n of the shunts is chosen to be equal for all shunts and defined so the EMCC for shunt 1 is $K^2_{c,11} = 0.02$. The EMCCs for the remaining shunts are shown in Table 1. The EMCC is decreasing for the shunts along the beam as the relative change of the target mode-shape decreases when transducers are placed gradually closer to the tip of the beam.

Table 1: EMCC for each shunt with all other shunts in SC.

Shunt	1	2	3	4	5
$K^2_{c,n}$	0.020	0.015	0.012	0.0078	0.0051

The effective stiffness coefficients are collected in a matrix $[1/\boldsymbol{\kappa}] = (1/\tilde{\kappa}_{kn})$ to illustrate the influence of the other shunts in the tuning of each shunt. Each element in the matrix is normalized with the corresponding diagonal elements such that $\sigma(a_{ij}) = a_{ij}/\sqrt{a_{ii}a_{jj}}$,

$$\sigma([1/\tilde{\boldsymbol{\kappa}}]) = \begin{bmatrix} 1.000 & -0.017 & -0.015 & -0.013 & -0.010 \\ & 1.000 & -0.013 & -0.011 & -0.009 \\ & & 1.000 & -0.009 & -0.008 \\ & & & 1.000 & -0.006 \\ & & & & 1.000 \end{bmatrix} \tag{32}$$

It is seen that the magnitude of the off-diagonal terms, which represent the modal coupling between the shunts, is between 0.6% and 1.7% compared to their respective diagonal elements. Although this coupling is small, it may be enough to distort the sensitive tuning for RL-shunts.

Each shunt is tuned based on the balanced tuning procedure in Section 3 with correction for all other shunts. The tuning is repeated individually for each shunt without correction for the other shunts, which corresponds to $\hat{\kappa}_n = \tilde{\kappa}_{nn}$ and $N_p = 1$. A root locus plot is shown for both cases in Figure 5 for varying values of the resistances R_n scaled by the same factor. Figure 5(b) shows that the balanced tuning leads to a root locus plot similar to the single shunt in Figure 4 except for four additional lines from the four added roots. The blue circles indicate the optimal tuning, whereas the blue triangles indicate that the reduction of the resistance by a factor $1/\sqrt{2}$ places two of the roots near the bifurcation point. For the individual tuning (a) it is seen that the red triangles do not meet at a bifurcation point, which indicates that the inductance is not balanced when neglecting the influence from other modes by the approximation $\hat{\kappa}_n = \tilde{\kappa}_{nn}$.

An FRF is shown for the rotation at the tip of the beam in Figure 5(c) and for the control force for each shunt in Figure 5(d). It is seen that the balanced tuning (blue) leads to a flat plateau, whereas the individual tuning (red) creates two distinct peaks with a substantial amplification at the low-frequency peak. This indicates that the presented tuning in Section 3 leads to a more flat plateau of response of the structure compared to individual tuning without proper balancing. Furthermore, it is seen that the proposed tuning gives a nearly identical and reduced force level for all shunts.

5 DISCUSSION AND FURTHER WORK

The system description in Section 2 shows that the influence from all shunts on the residual modes for a single shunt can be included in the force-displacement relationship. Furthermore, this coupling between the shunts can be described directly in terms of the modal electromechanical coupling coefficient (EMCC). The description of the coupling in terms of the modal EMCC improves the value of the representation, as it can be obtained in-situ without a detailed finite element model. The considered example shows the potential of including the influence from other shunts in the tuning of each shunt to obtain a more balanced tuning of the five parallel RL shunts on the cantilever. Other numerical tests have indicated that the proposed tuning method is sensitive to shunts located where the target mode has next to no relative deformation. This uncertainty – and a consistent model for optimal balance between the shunt force – will be addressed in future work.

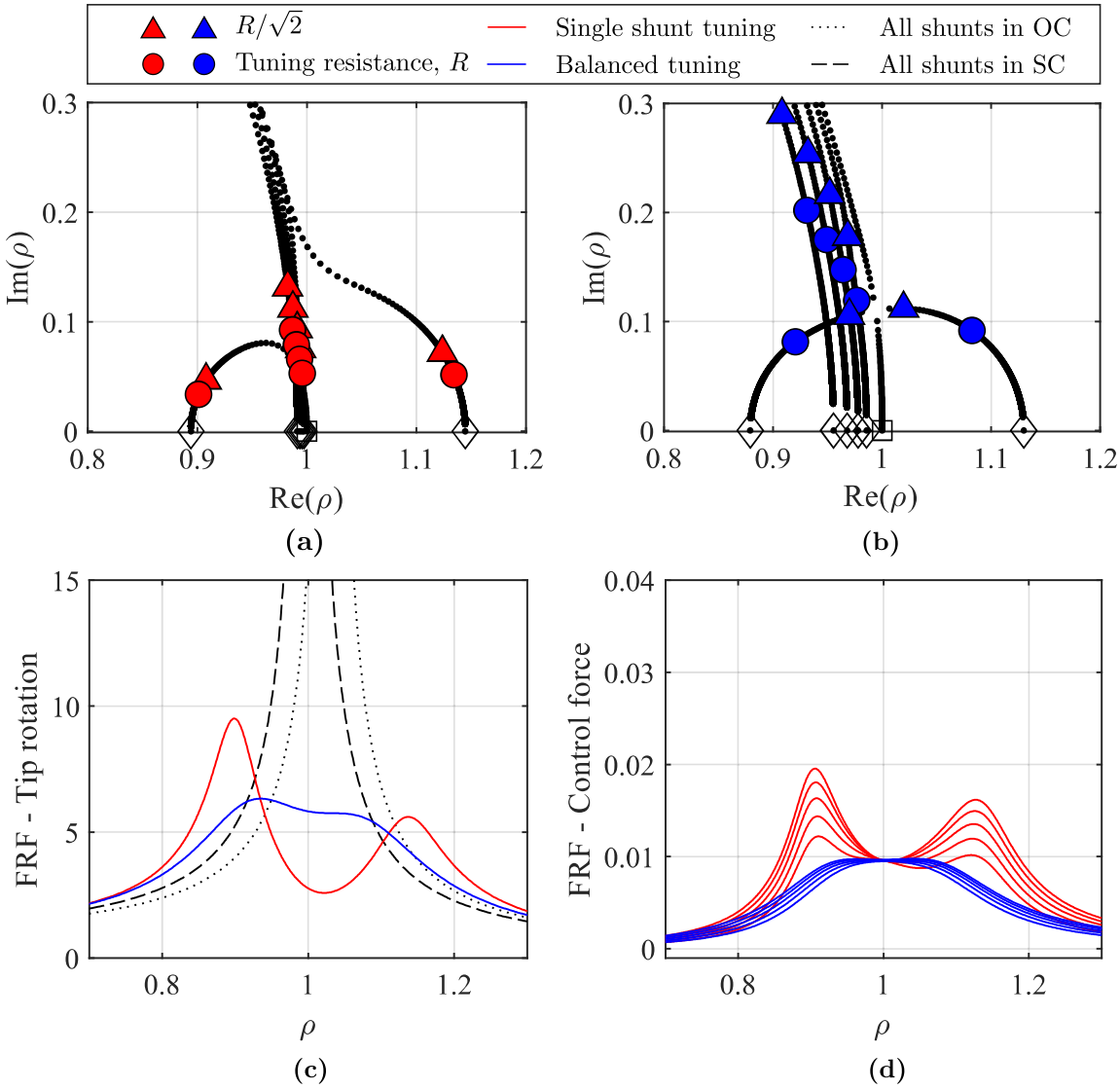

Figure 5: Root locus for (a) single and (b) balanced shunt tuning. FRF for (c) the rotation at the tip of the cantilever beam and (d) the force for the five shunts. The tuning resistance R (circle) corresponds to the resistance in (31) with $\hat{\kappa}_n = \tilde{\kappa}_{nn}$ and $N_p = 1$ for the single shunt tuning (red), whereas for the balanced shunt tuning (blue), $\hat{\kappa}_n = \sum_m \tilde{\kappa}_{nm}$ and $N_p = 5$.

References

[1] R. L. Forward, "Electronic damping of vibrations in optical structures," *Applied Optics*, vol. 18, no. 5, pp. 690–697, 1979.

[2] N. W. Hagood and A. von Flotow, "Damping of Structural Vibrations With Piezoelectric Materials and Passive Electrical Networks," *Journal of Sound and Vibration*, vol. 146, no. 2, pp. 243–268, 1991.

[3] S.-Y. Wu, "Piezoelectric shunts with a parallel R-L circuit for structural damping and vibration control," *SPIE*, vol. 2720, pp. 259–269, 1996.

[4] K. Yamada, H. Matsuhisa, H. Utsuno, and K. Sawada, "Optimum tuning of series and parallel LR circuits for passive vibration suppression using piezoelectric elements," *Journal of Sound and Vibration*, vol. 329, pp. 5036–5057, 2010. [Online]. Available: http://dx.doi.org/10.1016/j.jsv.2010.06.021

[5] J. Høgsberg and S. Krenk, "Calibration of piezoelectric RL shunts with explicit residual mode correction," *Journal of Sound and Vibration*, vol. 386, pp. 65–81, 2017. [Online]. Available: http://dx.doi.org/10.1016/j.jsv.2016.08.028

[6] M. Berardengo, O. Thomas, C. Giraud-Audine, and S. Manzoni, "Improved resistive shunt by means of negative capacitance: new circuit, performances and multi-mode control," *Smart Materials and Structures*, vol. 25, 2016.

[7] J. Høgsberg and S. Krenk, "Balanced calibration of resonant shunt circuits for piezoelectric vibration control," *Journal of Intelligent Material Systems and Structures*, vol. 23, no. 17, pp. 1937–1948, 2012.

[8] M. Geradin and D. J. Rixen, *Mechanical Vibrations - Theory and Application to Structural Dynamics*, 3rd ed. John Wiley & Sons Incorporated, 2015.

[9] A. Preumont, *Vibration Control of Active Structures*, 3rd ed. Springer, 2011. [Online]. Available: https://medium.com/@arifwicaksanaa/pengertian-use-case-a7e576e1b6bf

[10] A. Bloch, "Electromechanical analogies and their use for the analysis of mechanical and electromechanical systems," *Journal of the Institution of Electrical Engineers - Part I: General*, vol. 92, no. 52, pp. 157–169, 1945.

[11] S. Krenk, "Frequency analysis of the tuned mass damper," *Journal of Applied Mechanics - Transactions of the ASME*, vol. 72, no. 6, pp. 936–942, 2005.